A Study of Persistence in the Land–Atmosphere System with a Fourth-Order Analytical Model

YONGQIANG LIU AND RONI AVISSAR

Department of Environmental Sciences, Rutgers—The State University, New Brunswick, New Jersey

(Manuscript received 23 July 1997, in final form 24 June 1998)

ABSTRACT

In a companion paper, Y. Liu and R. Avissar analyzed the features of persistence in the land–atmosphere system simulated with the National Center for Atmospheric Research Community Climate Model Version 2 coupled with the Biosphere–Atmosphere Transfer Scheme (CCM2–BATS). To interpret the results obtained in that study, a fourth-order land–atmosphere analytical model is developed and used to investigate the timescales of disturbances in the land–atmosphere system, and the major parameters and processes affecting them. This analytical model has four damping timescales, namely seasonal, monthly, weekly, and daily. It is found that the seasonal scale is caused by self-feedback of soil moisture, and its length increases significantly due to the interactions between soil moisture and the other system variables. A sensitivity analysis performed with the Fourier amplitude sensitivity test indicates that the seasonal timescale is mostly affected by the physical parameters related to hydrological processes (namely, evaporation, runoff, and soil moisture diffusion), while the thermal characteristics of the land–atmosphere system mostly affect the monthly timescale. Thus, the results of this analytical study indicate that the persistence obtained in the CCM2–BATS simulation is an inherent property of the land–atmosphere system. They also emphasize the importance of soil moisture disturbances on persistence in the climatic system.

1. Introduction

To study persistence in the land–atmosphere system, Delworth and Manabe (1988, 1989, 1993) and Manabe and Delworth (1990) analyzed autocorrelations of monthly hydrological variables obtained from multiyear simulations with the Geophysical Fluid Dynamics Laboratory (GFDL) General Circulation Model (GCM). The ''bucket'' soil–water model developed by Manabe (1969) was used in this model. They found a significant persistence in soil moisture disturbances, especially at high latitudes, and during the winter season.

Applying a similar technique, Liu and Avissar (1999, hereafter LA99) analyzed the features of persistence in the land–atmosphere system simulated with the National Center for Atmospheric Research (NCAR) Community Climate Model Version 2 (CCM2) coupled with the Biosphere–Atmosphere Transfer Scheme (BATS) (hereafter CCM2–BATS). There are significant differences between BATS and the bucket model. For instance, unlike the bucket model, BATS accounts for the spatial distribution of different types of vegetation and soil. Also, it explicitly resolves soil temperature on a multilayer grid. LA99 claimed that these improved features provided new insights on persistence in the land–atmosphere system. For example, they found that persistence depends on regional climatology. It is stronger in the dry regions of North Africa and the inner-Eurasian continent than in their adjacent moist regions. This feature was supported by an analysis of soil and atmospheric observations in China. They also found that soil moisture has a much stronger persistence than soil temperature.

Two types of mechanism contribute to persistence in the land–atmosphere system: (i) external forcings, including the atmospheric dynamics that produce global circulation systems and control precipitation and cloudiness; and (ii) internal forcings, which consist of self-feedbacks and interactions within the system. Considering that GCMs need very large computing resources and account for a large number of complicated interactions often difficult to interpret, analytical models are good, efficient additional tools to study the mechanism of persistence.

Delworth and Manabe (1988) used a first-order Markov process model, in conjunction with simulations produced with the GFDL GCM, to study the timescale of decay of soil moisture disturbances. In that model, evaporation and precipitation are considered internal and external forcings, respectively. They showed that a sub-

Corresponding author address: Dr. Roni Avissar, Department of Environmental Sciences, Rutgers University, 14 College Farm Rd., New Brunswick, NJ 08901-8551.
E-mail: avissar@gaia.rutgers.edu

stantial part of the soil moisture variability occurs over a period of about 9 months in the Tropics to about 22 months at high latitudes. Furthermore, they indicated that the latitudinal dependence of persistence is probably caused by potential evaporation. Indeed, at high latitudes, where low potential evaporation results in slow dissipation of soil water, disturbances of soil moisture can easily persist for a relatively long time.

Delworth and Manabe (1988) pointed out that the first-order Markov process model is substantially similar to the bucket model used in the GFDL GCM. Thus, persistence obtained from the GFDL GCM simulations is explained quite well with this analytical model. But mainly because of the significant differences between BATS and the bucket model, a different analytical model is needed to explain the physical processes involved in persistence derived from CCM2–BATS simulations. First, in their analysis of persistence derived from a 10-yr CCM2–BATS simulation described in detail by Bonan (1994), LA99 found that, besides soil moisture, other components of the land–atmosphere system (namely, soil temperature, air humidity, and air temperature) also exhibit persistence. One can expect that disturbances in one of the components will affect the other components through various interactions and, as a result, affect their persistence. Therefore, to better understand the importance of soil moisture and soil temperature disturbances on the persistence in the entire land–atmosphere system, it is necessary to study these interactions. It is important to emphasize that first-order models, like the one used by Delworth and Manabe (1988), do not account for such interactions. Furthermore, one cannot explain the regional-climatology dependence of persistence found in the CCM2–BATS simulation with such a first-order model. This is because in that model the dissipation rate of soil moisture disturbances is determined by the ratio of potential evaporation to a constant water field capacity. The larger the ratio, the faster the dissipation. In dry regions, potential evaporation is large. Thus, the ratio is large and so is the dissipation rate. This suggests that the persistence of soil moisture is weaker in relatively dry regions. However, this contradicts the results of the CCM2–BATS simulation, implying that other important parameters affect persistence in the land–atmosphere system. Finally, various numerical experiments have shown that soil moisture anomalies can significantly affect local precipitation (e.g., Chen and Avissar 1994; Avissar and Liu 1996), emphasizing that precipitation is both an external and an internal forcing.

In this paper, a fourth-order land–atmosphere analytical model, which addresses the above issues, is developed to investigate which physical parameters and processes determine persistence in the land–atmosphere system. This model is described in the next section. In section 3, we use this model to analyze the timescales of persistence in the land–atmosphere system. In the following sections, we investigate the major factors affecting these timescales, as well as the feedbacks and interactions responsible for them.

2. The model

The model used for this investigation is an extension of the third-order model proposed by Liu et al. (1992). In that previous model, soil temperature, soil moisture, and air temperature are predicted, while variation of air humidity is assumed to compensate for the loss of water caused by variation in soil moisture. That model was used to study the role of soil moisture and vegetation on climate anomalies, and it indicated that the dissipation of disturbances grows faster as soil moisture and vegetation cover increase. However, there are two major problems with such a model. First, the interactions between soil moisture and air humidity are neglected. Second, the amplitude of the actual variations of soil moisture could be significantly reduced and, as a result, unrealistic estimates of the dissipation rate could be obtained.

In the model proposed here, in addition to the three variables included in the earlier model of Liu et al. (1992), air humidity is also introduced as a system variable. The equations describing the variations of the four variables represent a fourth-order model. Although it is no longer possible to obtain intuitive analytical solutions with such a higher-order model, it provides a very simple and inexpensive tool to study complex interactions in the land–atmosphere system, including those between soil moisture and air humidity.

In such a model, various types of parameters need to be specified to characterize, among others, the heat and water fluxes at the air–soil interface. A major improvement made to the present model is the derivation of these parameters from the above-mentioned CCM2–BATS simulation. In doing so, we expect these parameters to be specified consistently. Furthermore, this is also consistent with one of the objectives of this study, which consists of using the analytical results obtained here to interpret the features of persistence revealed by the CCM2–BATS simulation. It should also be pointed out that some of the schemes used by Liu et al. (1992) to calculate fluxes (including precipitation) are replaced with more appropriate schemes.

a. Equations

Figure 1 provides a diagram of the model, showing its structure, variables, and fluxes. To simplify the land–atmosphere system, the atmosphere is assumed to consist of an air column of height h_a. Its thermal and moisture states are characterized by its temperature, T_a, and its specific humidity, q_a. Noting that the soil depths at which thermal and hydrological processes are active are not necessarily identical, the soil is assumed to consist of a thermally active layer of depth d_T and a hydrologically active layer of depth d_Θ. Similar to the atmo-

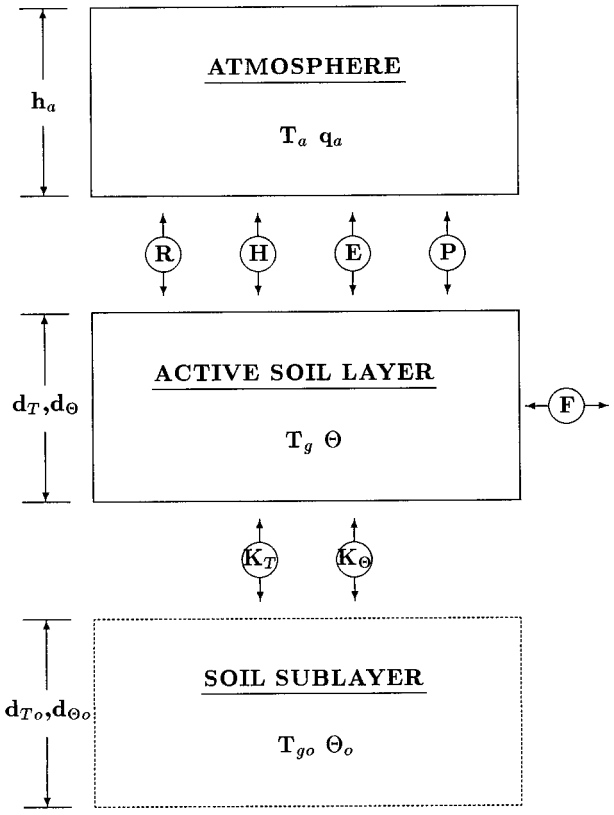

FIG. 1. A schematic representation of the land–atmosphere system (see appendix for list of symbols).

sphere, the soil is characterized by its temperature, T_g, and its volumetric soil water content, Θ. To account for possible diffusion of heat and moisture at the bottom of the active soil layers, soil sublayers of depth d_{To} and $d_{\Theta o}$ are defined for thermal and hydrological processes, respectively. Correspondingly, a constant temperature, T_{go}, and a constant volumetric soil water content, Θ_o, are assigned to these sublayers.

The fourth-order land–atmosphere system consists of the following set of heat and water conservation equations:

$$C_a \frac{dT_a}{dt} = R_a + H + LP, \tag{1}$$

$$M_a \frac{dq_a}{dt} = E - P, \tag{2}$$

$$C_g \frac{dT_g}{dt} = R_s - H - LE + K_T(T_{go} - T_g), \tag{3}$$

$$M_g \frac{d\Theta}{dt} = P - E - F + K_\Theta(\Theta_o - \Theta), \tag{4}$$

where $K_T = 2D_T C_g/[d_T(d_T + d_{To})]$ and $K_\Theta = 2D_\Theta M_g/[d_\Theta(d_\Theta + d_{\Theta o})]$; C_a $(=\rho_a c_p h_a)$ and C_g $(=\rho_g c_g d_T)$ are the heat capacity of the atmosphere and the soil, respectively (c_p is specific heat of air at constant pressure, c_g is specific heat of the soil, ρ is density, and subscripts a and g indicate atmosphere and ground); M_a $(=\rho_a h_a)$ and M_g $(=\rho_w d_\Theta)$ are masses of the air column and of a column of water of depth d_Θ per unit area, respectively; R_a and R_s are the radiation balance of the atmosphere and the land surface, respectively; H and E are the sensible heat flux and the moisture flux between the land surface and the atmosphere, respectively; P and F are precipitation and runoff, respectively; D_T and D_Θ are the soil thermal and hydraulic diffusivity, respectively; and L is the latent heat. It should be mentioned that land is assumed to completely cover the earth, and snow is neglected.

b. Fluxes

The radiative fluxes are calculated following Paltridge (1974):

$$R_s = [1 - \alpha_a(1 - n) - \alpha_c n - A_a - C_r n]S_o - \varepsilon\sigma T_g^4 + n\varepsilon\sigma T_a^4, \tag{5}$$

$$R_a = (A_a + C_r n)S_o + n\varepsilon\sigma T_g^4 - n\varepsilon\sigma T_a^4 - n\varepsilon'\sigma T_a^4 - (1 - n)G\sigma T_g^4. \tag{6}$$

The first term on the right-hand side of Eq. (5) is the net shortwave radiative flux at the land surface, where S_o is the incident shortwave radiation at the tropopause; α_a ($\approx$0.18) and α_c ($\approx$0.51) are the planetary albedo for clear sky and for cloudy atmosphere, respectively; A_a is the atmospheric absorption of shortwave radiation; and n is the cloud fraction. The next two terms together represent the net longwave radiative fluxes. The atmosphere is assumed to be opaque to longwave radiation at all wavelengths other than in the atmospheric window (7.5–12.5 μm), where absorption is assumed negligible. In this model, longwave energy transfer occurs only in the atmospheric window and, therefore, it is the only flux that needs to be considered. The constant σ is the Stefan–Boltzmann constant, and ε ($\approx$0.3) is the fraction of total blackbody radiation at normal earth temperatures contained within the wavelengths of the atmospheric window.

The first term on the right-hand side of Eq. (6) is the net shortwave radiative flux of the atmosphere. In this term, the factor C_r ($\approx$0.04) accounts explicitly for the extra shortwave absorption in clouds. The second and third terms represent the net longwave absorption in clouds resulting from exchange of radiant energy with the earth's surface. Again, only exchanges in the atmospheric window region of the spectrum are taken into account. It is assumed that the amount of water vapor above the level of the earth's cloudy regions is negligible. Thus, the window in the longwave spectrum has expanded to new limits, which are set only by the absorption bands of carbon dioxide. Accordingly, longwave loss to space from the clouds is given by $n\varepsilon'\sigma T_a^4$, where $\varepsilon' \approx 0.75$.

In clear atmosphere, the absorption bands of water vapor become less opaque with increasing height and decreasing water vapor concentration. In effect, the atmospheric window expands with increasing altitude so that each atmospheric level loses energy directly to space. Since the average temperature lapse to the tropopause is close to adiabatic as a result of mixing, on the average, the temperature at any level bears a fairly constant relation to the surface temperature. Thus, the total longwave loss from the clear-sky troposphere is likely to be proportional to surface blackbody radiation. This concept is the basis for the last term in Eq. (6), which contains a simple constant of proportionality G, which was found to be about 0.38 (on average) for a large number of studied typical cases. A detailed discussion of the philosophy behind this scheme, as well as of the values assigned to each of its variables, are given in Paltridge (1974).

The bulk flux formulas are used to calculate sensible heat and evaporation:

$$H = H_o(T_g - T_a), \tag{7}$$

$$E = \eta E_p = \eta E_o[q_s(T_g) - q_a], \tag{8}$$

where $H_o = \rho_a c_p C_{\mathrm{DT}} V$ and $E_o = \rho_a C_{\mathrm{DW}} V$; C_{DT} and C_{DW} are the sensible heat and moisture drag coefficients, respectively, which are strongly dependent upon land surface and atmospheric dynamic and thermal properties (e.g., vegetation cover and stability); V is the wind speed in the atmospheric surface layer; E_p is the potential evaporation; $q_s(T_g)$ is the saturated air specific humidity at temperature T_g; and $\eta = \Theta/\Theta_s$ is the soil wetness, with Θ_s being the volumetric soil water content at saturation. Note that the separate effect of the wind and the drag coefficient will not be considered here, and only their combined impacts, as measured by H_o and E_o, will be analyzed.

Both atmospheric dynamics and local moisture and heat exchanges in the land–atmosphere system can contribute to the essential conditions for the formation of precipitation (i.e., ascending motion of air mass, stratified instability, and water vapor supply). Because the model proposed here does not simulate atmospheric dynamics, precipitation is parameterized with a simple formula, which accounts only for the variances of atmospheric moisture and temperature caused by land–atmosphere interactions. This parameterization is based on the premise that at a given geographic location and a given general circulation pattern, precipitation is mostly related to the atmospheric water vapor content (W), and the relative humidity (R_h) of the entire air column. Applying dimensional analysis to relations between precipitation and these two factors, Fu (1978) developed the following formula:

$$P = C_1 W e^{-(C_2/R_h)^{C_3}}, \tag{9}$$

where C_i ($i = 1, 2, 3$) are empirical constants. In this model, $C_2 = 0.5$ and $C_3 = 4.5$, as suggested by Fu (1978). However, C_1 is derived from the ratio of climatological evaporation to precipitation (namely $r_{EP} = \overline{E}/\overline{P}$) derived from the CCM2–BATS simulation used by LA99.

TABLE 1. Parameters used in the coupled land–atmosphere system.

Parameter	Unit	Mean	Range in FAST*
T_a	K	255.0	250.0–260.0
q_a	g kg^{-1}	5.0	3.0–7.0
T_g	K	285.0	280.0–290.0
Θ	%	25.0	10.0–40.0
S_o	W m^{-2}	330.0	—
r_{EP}	%	60.0	45.0–75.0
n	%	50.0	35.0–65.0
d_T	m	10.0	0.75–1.25
d_{T_o}	m	10.0	—
d_H	m	1.0	0.75–1.25
d_{H_o}	m	10.0	—
h_a	km	10.0	9.0–11.0
D_T	m^2 s^{-1}($\times 10^{-7}$)	5.0	2.5–7.5
$D\eta$	m^2 s^{-1}($\times 10^{-8}$)	5.0	2.5–7.5
C_g	J K^{-1} m^{-3}($\times 10^6$)	1.0	0.75–1.25
Θ_s	%	40.0	30.0–50.0
H_o	W m^{-2} K^{-1}	1.0	0.5–1.5
E_o	kg m^{-2} s^{-1}($\times 10^{-3}$)	4.5	3.5–5.5
ρ_a	kg m^{-3}	0.75	—

* FAST stands for Fourier amplitude sensitivity test.

Runoff is proportional to the net soil water gain ($P - E$), and to the soil wetness (η):

$$F = \eta(P - E). \tag{10}$$

This type of relation is suitable for estimating runoff at the seasonal or longer timescales. Note that the parameter values used in this study (see Table 1), as well as the magnitude of the runoff perturbations, were selected to prevent negative runoff.

c. Perturbation equations

The perturbation approach (Holton 1979) is used to linearize the equations of the model. Accordingly, any variable ϕ is separated into a mean, $\overline{\phi}$, and a perturbation, ϕ'. Assuming that the perturbations are small as compared to the means, any terms including the product of two or more perturbations are assumed much smaller than terms including only one or no perturbation. Thus, for instance, the radiation emitted by a blackbody at a temperature T is given by $\sigma T^4 = \sigma(\overline{T} + T')^4 \simeq \sigma(\overline{T}^4 + 4\overline{T}^3 T')$. It should be noted that, in the real world, perturbations of clouds and precipitation can be larger than their average. But such perturbations are primarily related to atmospheric dynamics. However, in a model aimed at simulating the climatology of land–atmosphere moisture and temperature anomalies, one can expect that the standard derivation of clouds and precipitation will not be very large as compared to their mean.

The perturbation equations for the sensible heat and evaporation fluxes are

$$H' = H_o(T'_g - T'_a), \tag{11}$$

$$E' = \overline{\eta}E_o(\Delta_g T'_g - q'_a) + \overline{E}_p\Theta'/\Theta_s, \tag{12}$$

where $\Delta_g = dq_s/dT\,|_{T=\bar{T}_g}$.

To develop a perturbation equation for precipitation, we first substitute the atmospheric water content in Eq. (9) with the product of the specific humidity and the mass of the atmosphere, and the relative humidity with the ratio of the specific humidity to the specific humidity at saturation. Subsequently, we differentiate the expression and assume that the perturbation of a quantity is approximately equal to its differential value, and that the average is expressed by the nondifferential value. As a result, we obtain:

$$P'/\overline{P} = P_1 q'_a - P_2 T'_a, \tag{13}$$

where $P_1 = [1 + C_3(C_2/\overline{R}_h)^{C_3}]/\overline{q}_a$, $P_2 = C_3(C_2/\overline{R}_h)^{C_3}\Delta_a/\overline{q}_{as}$, and $\Delta_a = dq_s/dT\,|_{T=\bar{T}a}$.

The perturbation of cloud amount is related to the precipitation perturbation as follows:

$$n'/\overline{n} = P'/\overline{P}. \tag{14}$$

It should be noted that, in the real world, changes in cloudiness do not necessarily result in changes in precipitation (e.g., for nonprecipitating clouds).

The perturbation of the radiative fluxes is given by:

$$R'_s = (\varepsilon\overline{n}\Delta_{L_a} + R_{s1}P_2\overline{n})T'_a - \varepsilon\Delta_{L_g}T'_g - R_{s1}P_1\overline{n}q'_a, \tag{15}$$

$$R'_a = -(R_{a1} + R_{a3}P_2\overline{n})T'_a + R_{a2}T'_g + R_{a3}P_1\overline{n}q'_a, \tag{16}$$

where $R_{s1} = (\alpha_c - \alpha_a - C_r)S_o - \varepsilon\sigma\overline{T}_a^4$, $R_{a1} = (\varepsilon + \varepsilon')\overline{n}\Delta_{L_a}$, $R_{a2} = [(\varepsilon + G)\overline{n} - G]\Delta_{L_g}$, $R_{a3} = C_rS_o - (\varepsilon + \varepsilon')\sigma\overline{T}_a^4 + (\varepsilon + G)\sigma\overline{T}_g^4$, and $\Delta_{L_i} = d(\sigma\overline{T}_i^4)/dT_i$, $(i = a, g)$.

Using these flux perturbations, the heat and water conservation equations [Eqs. (1–4)] can be written:

$$\frac{d\mathbf{Y}}{dt} = C\mathbf{Y}, \tag{17}$$

where

$$\mathbf{Y} = (\mathbf{Y_i}) = (T'_a/\overline{T}_a,\ q'_a/\overline{q}_a,\ T'_g/\overline{T}_g,\ \Theta'/\overline{\Theta}), \tag{18}$$

$$\mathbf{C} = (c_{ij}) = \mathbf{l}_1\mathbf{A}\mathbf{l}_2. \tag{19}$$

Here, $\mathbf{l}_1$ is a diagonal matrix with elements $[(C_a\overline{T}_a)^{-1}, (M_a\overline{q}_a)^{-1}, (C_g\overline{T}_g)^{-1}, (M_g\overline{\Theta})^{-1}]$, $\mathbf{l}_2$, is a diagonal matrix with elements $[\overline{T}_a, \overline{q}_a, \overline{T}_g, \overline{\Theta}]$, and

$$\mathbf{A} = (a_{ij}) = \begin{bmatrix} -R_{a1} - H_o - (L\overline{P} + R_{a3}\overline{n})P_2 & (L\overline{P} + R_{a3}\overline{n})P_1 & R_{a2} + H_o & 0 \\ \overline{P}P_2 & -\overline{\eta}E_o - \overline{P}P_1 & \overline{\eta}E_o\Delta_g & \overline{E}_p/\Theta_s \\ \varepsilon\overline{n}\Delta_{L_a} + R_{s1}P_2\overline{n} + H_o & L\overline{\eta}E_o - R_{s1}P_1\overline{n} & -\varepsilon\Delta_{L_g} - H_o - L\overline{\eta}E_o\Delta_g - K_T & -L\overline{E}_p/\Theta_s \\ -\overline{\eta}_d\overline{P}P_2 & \overline{\eta}_d(\overline{P}P_1 + \overline{\eta}E_o) & -\overline{\eta}_d\overline{\eta}E_o\Delta_g & -\overline{\eta}_d\overline{E}_p/\Theta_s - \Delta_{PE}/\Theta_s - K_\Theta \end{bmatrix}, \tag{20}$$

where $\Delta_{PE} = \overline{P} - \overline{E}$, and $\overline{\eta}_d = 1 - \overline{\eta}$.

Equation (17) represents a set of linear, homogeneous differential equations with constant coefficients, whose linearly independent solutions can be written

$$Y_i(t) = \sum_{j=1}^{4} P_{ij}(t)e^{\lambda_j t}, \tag{21}$$

where $\lambda_j = (\lambda_r)_j + i(\lambda_i)_j$ $(j = 1, 4)$ are roots of the characteristic equation of Eq. (21), given by

$$\sum_{k=0}^{4} d_k\lambda^{4-k} = 0. \tag{22}$$

The parameter λ_r is the disturbance growth rate, and the reciprocal of its absolute value is the *e*-folding time. If $\lambda_r < 0$, the *e*-folding time is also called damping time [equivalent to the decay timescale in Delworth and Manabe (1988)], which is the time at which the amplitude of a disturbance is reduced to e^{-1} times its initial value. In Eq. (21), $P_{ij}(t)$ is a polynomial whose order is equivalent to the number of equal roots. In Eq. (22), d_k are constant coefficients, with $d_o = 1$ and $d_1 = -\sum_{k=1}^{4} a_{kk}$.

To provide the means of studying the impact of disturbances on the coupled land–atmosphere system, one could develop analytical solutions for this fourth-order model, as was done for the lower-order model of Liu et al. (1992). However, its solutions become cumbersome and no longer intuitive. Thus, a preferred alternative is the use of the eigenvalues of matrix **C**.

3. Timescales of disturbances

Table 1 lists the various atmospheric and soil conditions needed to calculate the elements of matrix **C**. These values are assumed to be representative of annual conditions under current climate over land. We adopted the values used in Paltridge (1974) for the radiative flux. The values of a few parameters related to other processes are taken from BATS (Dickinson et al. 1993) and from the results of the CCM2–BATS simulation per-

TABLE 2. Values of matrix $\mathbf{C} = (c_{i,j})$ ($\times 10^{-6}$).

	$j = 1$	$j = 2$	$j = 3$	$j = 4$
$i = 1$	−0.6410	0.0700	0.1171	0.0
$i = 2$	4.694	−1.708	19.79	0.6672
$i = 3$	1.673	0.0456	−9.178	−0.2195
$i = 4$	−0.2640	0.0961	−1.1130	−0.0883

TABLE 3. Damping times (in days) obtained from the real parts of the solutions of the fourth-order model.

Solutions	Decay times
1	231.5
2	57.5
3	5.7
4	1.2

formed by Bonan (1994). For instance, in BATS, the active soil layer is 1 m deep for 11 of the 16 land-cover types, and 1.5–2 m deep for the other types. The soil sublayer is 9 m deep for all land-cover types. Here these two layers are assumed to be 1 and 10 m deep, respectively. The spatially (over land) and temporally averaged ratio of evaporation to precipitation (r_{EP}) in the CCM2–BATS simulation is 0.60. The corresponding land surface sensible and latent heat fluxes are 33 and 61 W m^{-2}, respectively. Based on these values, as well as the climatological values of T_a, T_g, q_a, and η provided in Table 1, one can obtain H_o and E_o from Eqs. (7) and (8), respectively. A sensitivity analysis to H_o and E_o is given in section 4.

The resulting elements of matrix $\mathbf{C}$ are given in Table 2, and the solutions of the perturbation equations, which express damping times, are given in Table 3. The nature of the growth rate of disturbances is determined by the sign of the real parts of these solutions. It appears that all the solutions are real and negative, indicating that the initial disturbances in the system always decay with time. The damping time points out how fast disturbances decay with time. Consequently, it provides an essential information for understanding at which climatic scale a particular perturbation in the land–atmosphere system persists. A damping time of a few days implies that the considered perturbation is relevant to fast, synoptic-scale processes, but is unlikely to have a significant impact on longer timescales. On the other hand, a damping time of several months suggests a potential impact on seasonal climatic processes.

The damping times corresponding to the four solutions, as indicated in Table 3, are of the orders of 1 day, 1 week, 2 months, and 8 months. Thus, hereafter, they will be referred to as daily, weekly, monthly, and seasonal-scale processes, respectively. The monthly and seasonal scales, which represent long-term variations, will be referred to as long-term scales.

The long-term scale processes can be clearly seen from the evolution of the disturbances in the land–atmosphere system. Because all λ_j ($j = 1, 4$) are different, the order of P_{ij} (t) in Eq. (21) is zero. Denoting $P_{ij} = P_{ij}(t)$ and substituting Eq. (21) into Eq. (17), we have

$$\sum_{k=1}^{4} (a_{ik} - \delta_{ik}\lambda_j)P_{kj} = 0; \qquad i = 1, 4. \tag{23}$$

Here, δ_{ik} is the Kronecker Delta. For each λ_j, one can derive $P_{kj}(k = 1, 4)$ from this equation. Note, since λ_j is the eigenvalue of a_{ik}, $|a_{ik} - \delta_{ik}\lambda_j| = 0$. Thus, one of the four P_{kj} values remains unknown, and it is determined from the initial values of the system variables.

Three groups of simulations of four cases each were performed. In the first group, one perturbation at a time was imposed on the system (either air temperature, air humidity, soil temperature, or soil moisture). In the second and third group, two and four perturbations were imposed on the system, respectively. These perturbations are listed in Table 4. Their magnitude was derived from the standard deviation normalized by the mean values of air temperature and humidity at 700 hPa, and soil temperature and moisture obtained from the CCM2–BATS simulation, which are 1.54 K, 0.131 kg kg^{-1}, 2.1 K, and 0.046 m^3 m^{-3}, respectively. The evolution of the corresponding perturbed systems is illustrated in Fig. 2.

From the first group of simulations (cases GI1–GI4), it appears that when a perturbation of air temperature or air humidity is applied to the system, the system returns to its original state (i.e., the disturbance is almost completely damped) within a period of 6–8 months. A perturbation of soil temperature is damped within about 5 months, and a perturbation of soil moisture affects the system for about 1.5 yr. As illustrated in Fig. 2, typically, the system variables that were not originally perturbed reach a maximum disturbance within a period of a few weeks to a few months, and are then gradually damped.

Soil moisture is almost unaffected by disturbances of the three other variables. However, soil temperature is relatively strongly affected by soil moisture disturbances. A positive soil moisture disturbance of 5% results in a negative soil temperature perturbation of about −0.3 K. Air temperature is moderately affected by soil

TABLE 4. Initial perturbations in the land–atmosphere system.

Group	Case	$T'_a(K)$	$q'_a/\overline{q_a}$	$T'_g(K)$	Θ'/Θ
GI	1	1.5	0	0	0
	2	0	0.15	0	0
	3	0	0	2	0
	4	0	0	0	0.05
GII	1	1.5	0	2	0
	2	0	0.15	0	0.05
	3	1.5	0.15	0	0
	4	0	0	2	0.05
GIII	1	1.5	0.15	2	0.05
	2	−1.5	0.15	−2	0.05
	3	1.5	−0.15	2	−0.05
	4	−1.5	−0.15	−2	−0.05

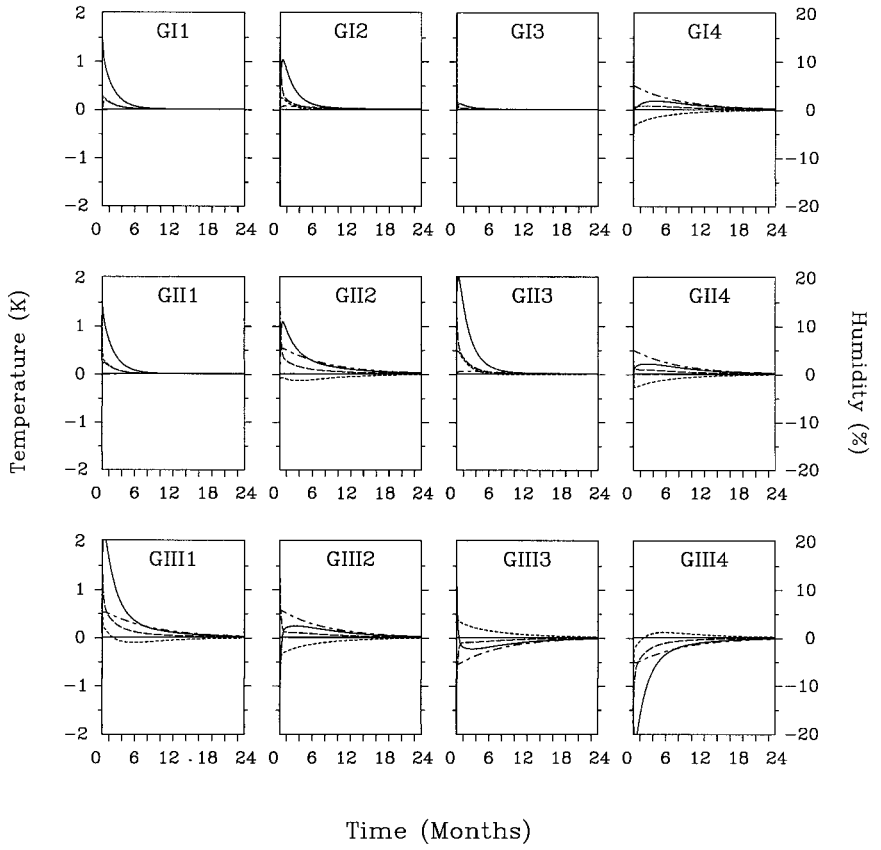

FIG. 2. Evolution of perturbations in the fourth-order land–atmosphere analytical model in response to the initial forcing listed in Table 4. The solid, dashed, dotted, and dashed–dotted lines represent the perturbations of air temperature (T'_a), normalized air humidity ($q'_a/\overline{q}_a$), soil temperature (T'_g), and normalized soil moisture ($\Theta'/\overline{\Theta}$), respectively.

temperature or soil moisture disturbances, and relatively strongly affected by air humidity perturbations. Air humidity is only moderately affected by disturbances of the three other variables.

The results of the second group of simulations (cases GII1–GII4) confirm the above results. The time needed by the coupled land–atmosphere system to damp the disturbances is equal to that of the longest of the two perturbations. Therefore, it is about 6–8 months for cases GII1 and GII3, and about 1.5 yr for cases GII2 and GII4. The sensitivity of each variable to perturbations of the three other variables is basically similar to cases GI1–GI4, and the magnitude of the perturbations is the sum of the individual perturbations.

It is interesting to note the strong impact of soil moisture perturbations on soil temperature. As can be seen from case GII4, even though a disturbance of +2 K was originally applied to the soil temperature, this perturbation very rapidly reaches a maximum negative value, similar to that resulting from the application of a soil moisture disturbance alone (case GI4).

Since in each of the third group of simulations (cases GIII1–GIII4) soil moisture perturbations are applied to the coupled land–atmosphere system, the damping of the perturbations takes about 1.5 yr. While these additional simulations confirm the results and conclusions discussed above, it is interesting to note the symmetry obtained by positive or negative perturbations, which is due to the linearity of the perturbation equations. Indeed, one can notice that case GIII1 is symmetric to case GIII4, and case GIII2 is symmetric to case GIII3. Thus, there is obviously no need to repeat the experiments illustrated in Figs. 2a–h with negative perturbations, as similar results, but with an opposite sign, would be obtained.

In summary, it appears that disturbances at the seasonal and longer timescales are obtained in all cases, and the longer disturbances are related to initial disturbances in soil moisture. The physical explanation to the importance of soil moisture is discussed in the following sections.

4. Which parameters affect the disturbances

The Fourier amplitude sensitivity test (FAST) is used to identify which parameters mostly affect the damping

times obtained from this fourth-order land–atmosphere model. This technique was introduced by Cukier et al. (1973) and was used, for example, by Uliasz (1988) to evaluate a Lagrangian long-range transport model, by Collins and Avissar (1994) to study the sensitivity of land surface heat fluxes to land surface characteristics, and by Liu and Avissar (1996) to examine sensitivity of shallow convective precipitation to atmospheric dynamic and cloud microphysical parameters.

In FAST, the input parameters are varied simultaneously through their ranges of possible values following their given probability density functions (i.e., values that have a greater probability are chosen more often). All input parameters are assumed to be mutually independent and each is assigned a different frequency, which determines the number of times that the entire range of values is traversed. With each input parameter oscillating at a different characteristic frequency, a different set of input parameter values is obtained for each model run with every value used once. The mean and variance, which characterize the uncertainty due to the variability of the input parameters, are calculated for model output parameters. Fourier analysis of each output for all model runs is used to separate the response of the model to the oscillation of particular input parameters. Summation of those Fourier coefficients corresponding to a particular input parameter frequency and its harmonics determines the contribution of that input parameter to the model output variances. Finally, by scaling the relative contribution of the input parameters to the total variance, partial variances are obtained, which show the sensitivity of model output parameters to the variation of individual input parameters in terms of a percentage of the variance.

The Fourier coefficients corresponding to input parameter frequencies and their harmonics do not account for the total variance of the model outputs. The Fourier coefficients corresponding to linear combinations of more than one input parameter frequency account for the remaining percentage of the variance, which can be attributed to the combined influences of two or more parameters.

In comparison to other techniques [e.g., Monte Carlo, Latin hypercube sampling (McKay et al. 1979; Derwent 1987)], the advantages of this technique are evident considering that, for instance, it requires only 1027 runs for a model with 15 input parameters. For comparison, if 10 values would be used within the range of all input parameters, a total of 10^{15} model runs would be needed with a stratified sampling technique. Moreover, FAST provides information on the model sensitivity to particular input parameters, unlike other techniques for sensitivity analysis. A complete description of the theory and implementation of FAST and approximations used in computer implementation, mainly following Cukier et al. (1978) and Uliasz (1988), is given in Collins and Avissar (1994) and Liu and Avissar (1996).

Fifteen out of the 19 input parameters of our fourth-order model listed in Table 1 were chosen for this analysis. Normal distributions of these input parameters were considered, and their ranges are also given in Table 1. Note that, as required in FAST, the 15 parameters selected here were defined independently of each other. However, it should be emphasized that, in fact, some of them are physically related. For instance, this is the case for clouds, and air temperature and air humidity.

Figure 3 depicts the partial variance of the damping times resulting from this sensitivity test. It appears that the longest damping timescale, which is about 9.5 months, is very sensitive to soil moisture, the ratio of evaporation to precipitation, soil temperature, and soil moisture at saturation. Each of these parameters contributes more than 10% to the total variance. In addition, the drag coefficient of the water vapor flux, the depth of the hydrologically active soil layer, air humidity, and soil hydraulic diffusivity have some impact on the variance. It is interesting to note that all these parameters are related to soil hydrological processes. Indeed, the ratio of Θ to Θ_s affects the actual evaporation; E_o, T_g, and q_a affect the potential evaporation; r_{EP} is related to evaporation and precipitation; and D_Θ and d_Θ affect the transfer of water between the active soil layer and the soil sublayer. Thus, clearly, the parameters associated with soil hydrology determine the length of the longest process in the land–atmosphere system.

The cloud fraction, whose partial variance contributes more than half of the total variance, has the dominant impact on the monthly damping timescale. Note, clouds in this model are ''passive,'' that is, they are related to precipitation, and they only affect temperature through radiative fluxes. Therefore, here they are considered a thermal property of the atmosphere, while in fact they are both thermal and hydrological properties. In addition to the cloud fraction, the air column height and the air temperature each contribute 10%–15% to the total variance. Thus, it can be concluded that the monthly timescale is mostly affected by the thermal properties of the atmosphere.

The weekly damping timescale is mostly affected by the parameters that control evaporation. As clearly depicted in Fig. 3c, q_a, T_g, Θ, and E_o contribute together about 80% of the total variance. Finally, the daily damping timescale is mostly affected by soil moisture (Fig. 3d), but it is important to note that soil thermal properties also have a significant impact on this timescale.

5. Impact of the major parameters on damping timescales

Based on the FAST analysis presented in the previous section, we examine the effects of the five most important parameters (at each timescale) on the damping timescales. The range considered for each parameter is the same as in the previous experiments (see Table 1).

Figure 4 shows that, at the seasonal scale, the five considered parameters can have a very strong impact

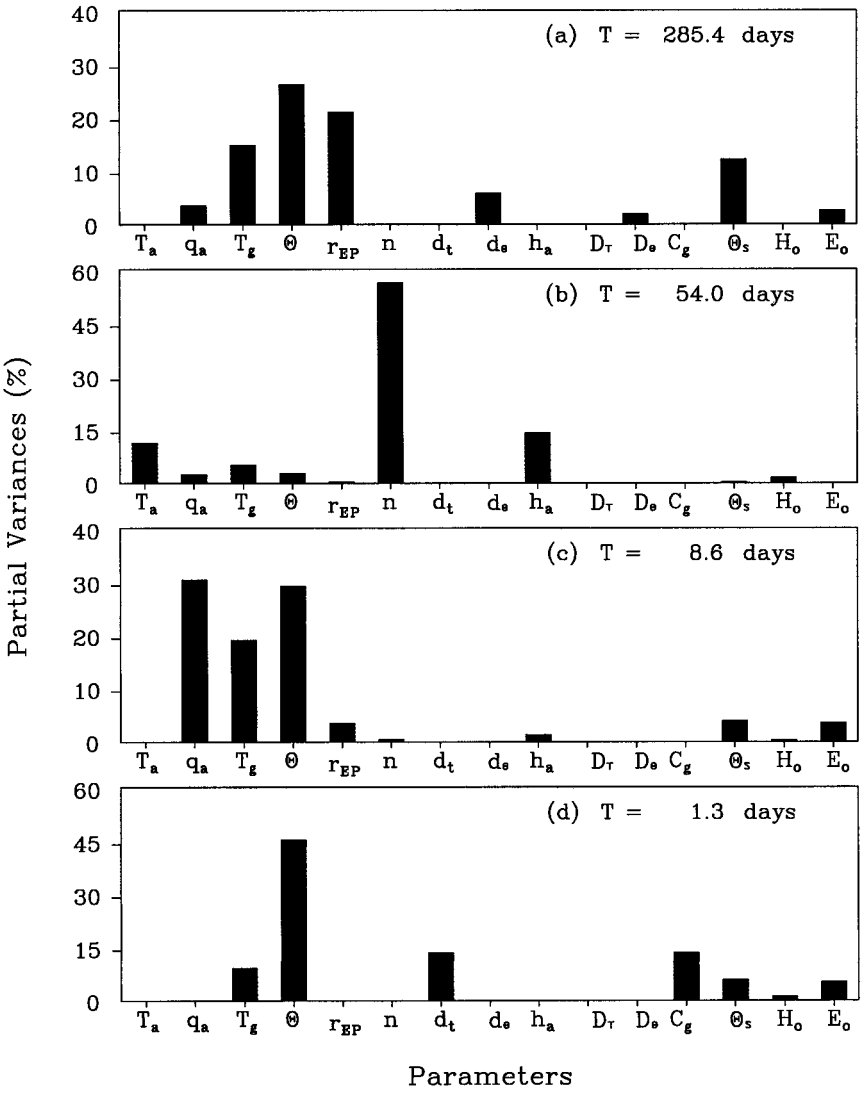

FIG. 3. FAST of the fourth-order model outputs: (a) seasonal, (b) monthly, (c) weekly, and (d) daily damping timescales, as indicated by the average timescale (T) obtained from all model runs. Partial variances reflect sensitivity of the timescales to the model inputs (see appendix for list of symbols).

on the damping timescale. For instance, a dry soil ($\Theta = 0.1$) has a damping time of 485 days, but a wet soil ($\Theta = 0.4$) has a damping time of only 153 days, emphasizing that a moist soil damps a perturbation much faster than a dry soil does. An increase of 10°C in soil temperature causes a reduction of 6 months in the damping time (from 364 to 156 days), and an increase of E_o (which is proportional to the turbulence activity in the atmospheric surface layer) from 3.5 to 5.5 $\times$ 10^{-3} kg m^{-2} s^{-1}, results in a reduction of the damping time from 283 to 196 days. When r_{EP} and Θ_s increase, they result in a very significant increase of the damping time.

The evaporation equation [Eq. (8)] consists of two variables, namely potential evaporation (E_p) and soil wetness (η). Here E_p increases with T_g and E_o, and decreases with q_a. Therefore, it can be assessed from the relations between these three parameters and the damping time (Fig. 4), that the damping timescale decreases with an increase in potential evaporation. The relations between the damping time and Θ and Θ_s indicate that the damping time decreases with η. The combined effects of E_p and η result in a decrease of the damping time with an increase in actual evaporation.

The runoff parameterization [Eq. (10)] consists of two variables as well, that is, η, and the net soil water gain ($P - E$). The later is inversely proportional to r_{EP}. Figure 4 shows that the damping time increases from 138 to 393 days with a variation of r_{EP} from 0.45 to 0.75 or, equivalently, decreases with ($P - E$). Therefore,

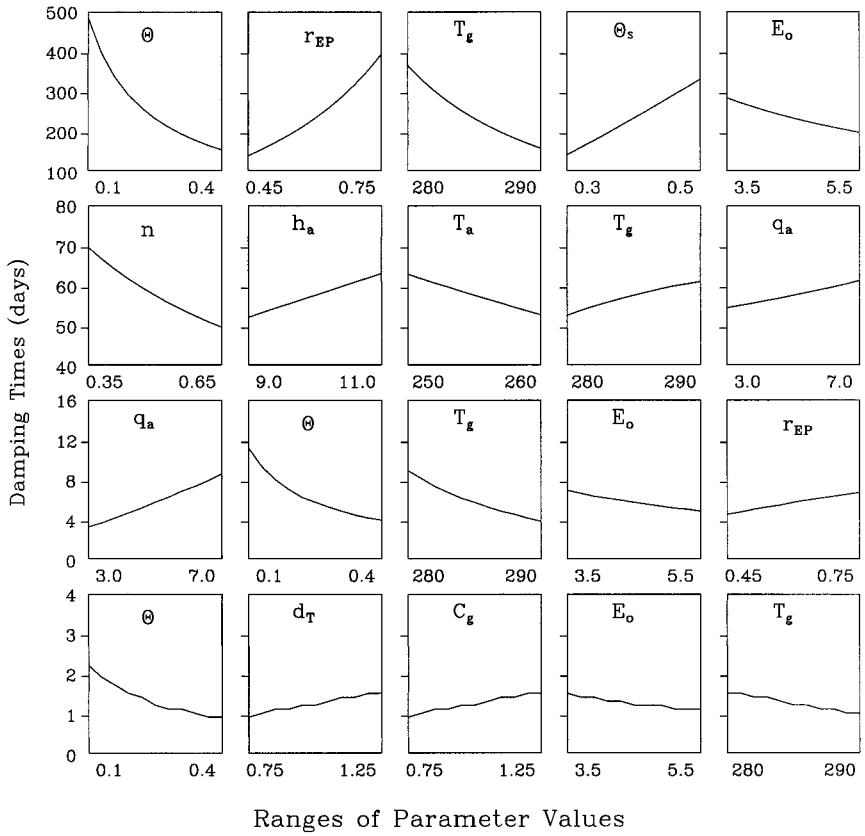

FIG. 4. Sensitivity of the damping times to the major physical parameters of the fourth-order land–atmosphere analytical model (see appendix for list of symbols).

together with the variation of η, the damping time decreases with an increase in runoff.

The last term on the right-hand side of Eq. (4) is the exchange of soil moisture between the active layer and the sublayer, which acts as a force-restore term for soil moisture disturbances. Its intensity is proportional to D_Θ and inversely proportional to d_Θ. The damping time decreases with D_Θ and increases with d_Θ (not shown). Therefore, it decreases with a faster exchange between the two soil layers. Here d_Θ is also a measure of the total available water in the active layer. For a given forcing, as expressed by the right-hand side terms in Eq. (4), the larger d_Θ, the slower the variation rate of soil moisture, and the longer the damping time. This effect is somewhat similar to that of soil heat capacity in damping the variation of soil temperature. However, evaporation and runoff affect the damping time much more significantly than the exchange between the two soil layers does.

In summary, the smaller the fluxes of water in the land–atmosphere system (i.e., evaporation, runoff, and underground diffusion) are, the longer the damping time is, and, therefore, the more significant persistence is.

The monthly scale is significantly affected by the five parameters considered here: it decreases with the increase in cloudiness and air temperature, and increases with the increase in the three other parameters. As can be seen in Fig. 3, cloudiness is a dominant factor contributing to the total variance at this timescale, and Fig. 4 indicates that the damping time decreases from 70 to 49 days as cloudiness increases from 0.35 to 0.65. This parameter affects the radiation balance of both the atmosphere and the ground surface. It appears that an increase in cloudiness results in an increase of the overall radiation balance, and a greater energy exchange rate in the land–atmosphere system. As a result, the dissipation of disturbances is faster.

Four of the five parameters, which have significant effects on both the weekly and the seasonal scales, are common. The other one, namely, air humidity, results in an increase of the weekly damping time by 6 days, when it increases from 0.03 to 0.07. This increase is apparently caused by a reduced evaporation from the land surface in a moister atmosphere. The daily scale decreases with an increase in Θ, E_o, and T_g, and increases with an increase in d_T and C_g.

It should be noted that the above sensitivity analysis is not able to directly illustrate how the solar radiation contributes to the damping times, because the latent and sensible heat fluxes have been prescribed separately,

TABLE 5. Damping times (in days) obtained from the real parts of the solutions of the third-order models.

Solutions	$T'_a = 0$	$q'_a = 0$	$T'_g = 0$	$\Theta' = 0$
1	229.4	195.6	235.6	58.1
2	7.3	18.7	29.1	5.7
3	1.2	1.3	5.8	1.2

TABLE 6. Damping times (in days) obtained from the real parts of the solutions of the second-order models.

Solutions	$T'_g = \Theta' = 0$	$T'_a = q'_a = 0$	$q'_a = \Theta' = 0$	$T'_a = T'_g = 0$
1	29.6	188.2	18.7	233.0
2	5.9	1.3	1.3	6.6

without any constraint on the balance between the surface net radiation and the two fluxes (an advantage of doing so is the possibility to examine independently the relative contribution of air and soil parameters to persistence). But using the Bowen ratio together with solar radiation, this sensitivity can be examined. For that purpose, we first relate the heat and water vapor drag coefficients, C_{DT} and C_{DW}, to the Bowen ratio β:

$$\beta = \frac{\overline{H}}{L\overline{E}} = \frac{c_p C_{DT}(\overline{T}_g - \overline{T}_a)}{LC_{DW}\overline{\eta}[q_s(\overline{T}_g) - \overline{q}_a]} \tag{24}$$

giving

$$C_{DT} = C_{DW}\beta\left[\frac{L\overline{\eta}[q_s(\overline{T}_g) - \overline{q}_a]}{c_p(\overline{T}_g - \overline{T}_a)}\right]. \tag{25}$$

Assuming balance between climatic net radiation, sensible heat flux, and latent heat flux, we obtain:

$$C_{DW} = \frac{\overline{R}_s + K_T(\overline{T}_{go} - \overline{T}_g)}{\rho_a LV\overline{\eta}[q_s(\overline{T}_g) - \overline{q}_a](\beta + 1)}. \tag{26}$$

The sensitivity analysis of the longest damping time to the solar radiation (S_o) indicates that the damping time decreases from about 295 to 206 days as S_o increases from 300 to 380 W m^{-2}.

6. Major physical processes

a. Processes responsible for the various timescales

The evolution of the disturbances in the land–atmosphere system is controlled by two mechanisms: self-feedbacks, which are measured by the four diagonal elements in matrix **C** [Eq. (19)], and interactions, which are measured by the 12 other elements of that matrix. The physical processes responsible for each of the four damping timescales can be analyzed by examining the behavior of the various lower-order systems, which can be derived from the fourth-order model by excluding the feedbacks and interactions caused by one or more system variable(s).

Four third-order systems are obtained by eliminating one of the four system variables at a time in Eqs. (1)–(4) (i.e., $T'_a = 0$, $q'_a = 0$, $T'_g = 0$, or $\Theta' = 0$). The resulting damping times are presented in Table 5. They indicate that the seasonal damping timescale appears only in the third-order systems with disturbance of soil moisture. The longest damping time in the first three systems varies between 196 and 236 days. This emphasizes that the soil moisture feedback, and its interactions with the other variables, are the primary cause for the damping timescale. In the third-order system without physical processes related to soil moisture disturbances, the maximum damping timescale is only of the order of two months. In addition, among the various interactions, the one between soil moisture and air humidity is the predominant: excluding this interaction results in a reduction of the damping time from 232 to 196 days. On the other hand, the exclusion of the interactions involving air and soil temperature has little impact on the damping timescales.

Four second-order systems were considered here: (i) $T'_g = \Theta' = 0$, (ii) $T'_a = q'_a = 0$, (iii) $q'_a = \Theta' = 0$, and (iv) $T'_a = T'_g = 0$. The damping times obtained with these second-order systems are presented in Table 6. With system (i), which does not account for soil-variable perturbations, the disturbances sustain for a period of about one month. However, a damping time of about 6 months is obtained with system (ii), which does not account for air-variable perturbations. Considering these results and those obtained with the third-order systems, it seems that atmospheric disturbances can persist on the seasonal scale only if there are interactions between atmospheric variables and soil moisture. The other two second-order systems further illustrate the importance of the moisture processes. Clearly, thermal disturbances have a short-time impact on the land–atmosphere system, while moisture disturbances persist for as long as 8 months.

Assuming that there are no interactions among the four system variables, Eqs. (1)–(4) become four independent first-order systems. Each one contains only one of the four perturbation variables. Obviously, in these cases, the variation of the disturbances in the systems is caused by self-feedback. The results show that the damping time is about 3.5 months for the first-order system, which accounts for soil moisture perturbations, and several days to three weeks for the other systems.

Three major conclusions can be drawn from the damping times obtained with the different systems discussed here. First, results from the first-order systems indicate that self-feedbacks are the primary mechanisms for the formation of the timescale of persistence. Specifically, soil moisture feedback causes seasonal-scale persistence. Second, the interactions between soil moisture and the other variables of the land–atmosphere system (mainly air humidity) cause a significant increase of the long-term persistence, from about 3.5 months

when only soil moisture self-feedback is considered, to about 8 months when various interactions are introduced in the land–atmosphere system. Finally, for atmospheric disturbances to persist at the seasonal scale, interactions between the atmosphere and soil moisture must be considered.

Note, the intensity of the soil moisture feedback is mainly controlled by the various hydrological fluxes (i.e., evaporation, runoff, and water diffusion between the two soil layers), as shown in matrix **C**. Thus, this confirms the importance of these fluxes on long-term disturbances, which was already found in the sensitivity analysis described in section 4.

b. Processes responsible for the disturbance decay

In section 3, we indicated that disturbances in the land–atmosphere system tend to dissipate with time (i.e., they have negative growth rates). Here we examine the role of feedbacks and interactions on the rates of dissipation.

The four diagonal elements of matrix **C** are negative. Thus, their sum and average are also negative. From the relation between roots and coefficients derived from Eq. (22), namely, $\Sigma\, \lambda_k = -d_1/d_o = \Sigma\, a_{kk}$, it appears that the average of the roots, which is equal to the average of the four diagonal elements of matrix **C**, is also negative. The diagonal elements of matrix **C** represent the self-feedbacks of the land–atmosphere system. A negative value indicates a negative self-feedback, which results in disturbance decay.

A physical explanation to the roles of these self-feedbacks can be given by using the perturbation equations. For instance, a positive perturbation of air temperature results in a decrease of sensible heat released in the atmospheric surface layer from the land surface, and in an increase of heat lost by longwave radiation. Consequently, one can expect a decrease in precipitation, which results in a reduced release of condensation latent heat, due to the corresponding lower relative humidity. These effects induce a negative air temperature tendency. Similarly, a positive perturbation of soil temperature results in an increase in heat loss to the atmosphere by sensible heat flux, latent heat flux, and longwave radiation, and into the soil sublayer by conduction, which leads to a decrease in soil temperature. A positive perturbation of air moisture results in a decrease of the amount of water evaporated from the land surface and, possibly, in an increase in condensation, which removes vapor from the atmosphere. Finally, a positive perturbation of soil moisture results in an increase in evaporation to the atmosphere, in runoff, and in the amount of water lost by percolation to the soil sublayer.

But there are also positive interactions in the system, as indicated by the positive elements of matrix **C**, which can promote the growth of disturbances. For example, a positive perturbation of soil moisture results in a more humid atmosphere due to a stronger evaporation at the land surface, and a moister atmosphere is likely to produce more precipitation, which in turn increases soil moisture.

Eventually, the overall evolution of the disturbances (i.e., amplification or decay) depends on the relative importance of the feedbacks and interactions. Because all the roots of the coupled land–atmosphere system (and their mean) are negative, disturbances decay with time. Thus, one can expect that self-feedbacks have a predominant impact on this system.

The fourth-order system is too complicated to provide a clear and intuitive analysis of the contribution of the feedbacks and interactions to the overall behavior of the coupled land–atmosphere system. Thus, a second-order model of the land–atmosphere system, which contains the major processes affecting long-term disturbances, is used here. Note, this model, which is based on the perturbation equations of soil and atmospheric moisture, can be analytically solved. Denoting its coefficient matrix as **B**, its four elements are $b_{11} = a_{22}$, $b_{12} = a_{24}$, $b_{21} = a_{42}$ and $b_{22} = a_{44}$. The characteristic equation of this system is given by

$$\lambda^2 + b\lambda + c = 0, \tag{27}$$

where

$$b = -(b_{11} + b_{22}) \tag{28}$$

and

$$c = b_{11}b_{22} - b_{12}b_{21}. \tag{29}$$

Solutions of this equation are

$$\lambda_{1,2} = (-b \pm \Delta)/2, \tag{30}$$

where $\Delta = (b^2 - 4c)^{1/2}$.

A sufficient condition for the equation to have two different, negative, real roots, which ensures that disturbances in the second-order system decay with time, is $b > 0$, $c > 0$, and $\Delta > 0$. Because both self-feedbacks b_{11} and b_{22} are negative, $b > 0$. Also,

$$\Delta > [(\overline{\eta}E_o + \overline{P}P_1) - (1 - \overline{\eta})\overline{E}_p\Theta_s^{-1}]^2 > 0. \tag{31}$$

Note that $\overline{P} > \overline{E}$ is assumed for obtaining this relation.

The determinant of matrix **B** (namely, c) is equal to the difference between the product of the two self-feedbacks and the product of the two interactions, both of which are greater than zero. Thus, its sign is an indicator of the relative importance of the feedbacks and interactions in the system: A positive value indicates a dominant role of the feedback, while a negative value emphasizes that the interactions are dominant. From the second-order system, one obtains:

$$c = (\delta_{PE}/\Theta_s + K_\Theta)(\overline{\eta}E_o + \overline{P}P_1) > 0 \tag{32}$$

emphasizing that self-feedbacks are always dominant and that disturbances decay with time.

7. Conclusions

A fourth-order land–atmosphere model based on perturbation equations obtained from heat and water conservation principles in the soil and the atmosphere was developed to study persistence in the coupled land–atmosphere system. The following major results are obtained from this study.

1) The land–atmosphere system has seasonal, monthly, weekly, and daily damping timescales. This suggests that disturbances in this system could persist for seasons. Thus, persistence is an inherent property of the land–atmosphere system. This result provides theoretical support to the studies of Namias (1952, 1959) and others, who indicated that atmospheric anomalies possess month-to-season persistence.

2) The seasonal damping timescale is due to the soil moisture self-feedback, and interactions between soil moisture and the other variables of the system greatly increase the damping timescale. When soil moisture processes are ignored, disturbances in the land–atmosphere system decay rapidly. Thus, this study provides theoretical support to Namias' assumption (1959) that land is a primary factor affecting persistence.

3) The seasonal damping timescale is mostly affected by the physical factors related to soil moisture (i.e., evaporation, runoff, and soil moisture diffusion), and the monthly damping timescale is mainly affected by the thermal characteristics of the system.

In a companion paper Liu and Avissar (1999) examined persistence in a simulated land–atmosphere system with the NCAR CCM2 coupled with BATS, and in observations of soil and atmospheric variables in China. They also showed that soil moisture and soil temperature perturbations persist for months to seasons, and that soil moisture persistence is much stronger. That investigation provides support to this analytical study. Persistence timescales of months to seasons were also obtained in a number of other numerical and observational studies (e.g., Walker and Rowntree 1977; Rind 1982; Rowntree and Bolton 1983; Yeh et al. 1984; Walsh et al. 1985; Liu et al. 1993; Gao et al. 1996; Vinnikov et al. 1996).

This study clearly emphasizes the importance of considering hydrological processes in general, and soil moisture in particular, in climatic studies at monthly and seasonal timescales. This conclusion has been pointed out by other investigators. For instance, Castelli and Rodriguez-Iturbe (1995) found that land–atmosphere interactions can influence local atmospheric processes through the modification of the vertical lapse rate, and large-scale processes through the global dynamics of baroclinic waves. The advection rates of mass and energy, and the strength of the ageostrophic frontal circulations are particularly important in that case. Betts et al. (1996) showed that the monthly precipitation pattern is quite sensitive to initial soil moisture in the First International Satellite Land Surface Climatology Project Field Experiment and Boreal Ecosystem–Atmosphere Study experiments. They suggested that, due to the memory of the soil moisture reservoir, some predictability exists at monthly and seasonal scales. Avissar (1995) emphasized the importance of an appropriate representation of soil moisture in global climate models.

While the results presented in this paper provide significant insights on the importance of land–atmosphere interactions on the prediction of atmospheric processes at monthly and seasonal scales, it is important to keep in mind that only small-amplitude disturbances in a linear system were considered here. One obvious limitation with such a model is that it neglects scale interactions in the climate system. In the real world, however, short-time forcings can generate long-time fluctuations. The relation between tropical convection activity, 30–60-day low-frequency fluctuations, and the El Nino–Southern Oscillation is but one example of such interactions. The possible relations between the daily, weekly, monthly, and seasonal scales in the model need to be examined with nonlinear models. Additional simulations with GCMs and analyses of nonlinear behaviors of the land–atmosphere system are likely to provide additional insights on this important issue.

The fourth-order analytical model developed here does not have positive growth modes. Two factors contribute to this. First, the model does not have external forcing related to, for example, atmospheric dynamics, which causes disturbances in the land–atmosphere system. Second, the nature of the development of the system (i.e., growth or decay) depends very much on the model parameters. In this study, climatological values have been given to these parameters. Thus, the results presented here reflect the climatological behavior of the land–atmosphere system. However, the model could give solutions, which indicate growing disturbances, by selecting specific sets of parameters reflecting local, short-term conditions. In addition, due to the lack of atmospheric dynamics, this model is unable to address the potentially important role of atmospheric systems (e.g., blocking or other standing waves) on atmospheric persistence.

Finally, snow has a major impact on the land–atmosphere interactions at mid- and high-latitudes during winter time. It can significantly affect soil moisture and, as a result, persistence in the entire land–atmosphere system. But snow is not represented in the model used here. Therefore, a more detailed model including snow processes would probably provide additional insights on persistence in the land–atmosphere system.

Acknowledgments. We would like to thank Alan Robock and the anonymous reviewers for valuable suggestions and comments, which contributed to improve our manuscript. This research was supported by the National Oceanic and Atmospheric Administration under Grant NA56GP0200, by the National Aeronautics and Space Administration under Grant NAG8-1513, and by

the National Science Foundation under Grant EAR-9415441. The views expressed herein are those of the authors and do not necessarily reflect the views of these agencies.

APPENDIX

List of Symbols

a_{ij}	Elements of matrix **A**
A	Coefficient matrix of the fourth-order perturbation model
A_a	Atmospheric absorption of shortwave radiation
b_{ij}	Elements of matrix **B**
B	Coefficient matrix of the second-order perturbation model
c_g	Specific heat of soil
c_{ij}	Elements of matrix **C**
c_p	Specific heat of air at constant pressure
C_a	Heat capacity of atmosphere
$C_{\rm DT}$	Sensible heat drag coefficient
$C_{\rm DW}$	Water vapor drag coefficient
C_g	Heat capacity of soil
C_k	Empirical constant for calculating precipitation ($k = 1, 2, 3$)
C_r	Cloud absorption of shortwave radiation
d_T	Depth of thermally active soil layer
d_{To}	Depth of thermal soil sublayer
d_Θ	Depth of hydrologically active layer
d_{Θ_o}	Depth of hydrological soil sublayer
D_T	Soil thermal diffusivity
D_Θ	Soil hydraulic diffusivity
E	Evaporation
E_o	Turbulent water vapor exchange index
E_p	Potential evaporation
F	Runoff
G	Ratio of clear-sky longwave radiative loss to the surface longwave radiation
h_a	Height of air column
H	Sensible heat flux
H_o	Turbulent sensible-heat exchange index
K_T	Soil thermal conductivity
K_Θ	Soil hydraulic conductivity
L	Latent heat
M_a	Mass of atmosphere
M_g	Mass of soil
n	Cloud fraction
P	Precipitation
P_{ij}	Polynomials in the characteristic equation of the fourth-order model
P_k	Precipitation function ($k = 1, 2$)
q_a	Air specific humidity
q_s	Air specific humidity at saturation
r_{EP}	$\overline{E}/\overline{P}$
R_a	Atmospheric radiation flux
R_{ak}	Atmospheric radiation function ($k = 1, 2, 3$)
R_h	Relative humidity
R_s	Radiative flux at the ground surface
R_{s1}	Surface radiation function
S_o	Solar radiation at tropopause
T_a	Air temperature
T_g	Soil temperature
T_{go}	Soil sublayer temperature
V	Wind speed
W	Atmospheric water content
α_a	Clear-sky albedo
α_c	Cloudy atmosphere albedo
β	Bowen ratio
δ_a	$dq_s/dT\,\vert_{T=\bar{T}_a}$
δ_g	$dq_s/dT\,\vert_{T=\bar{T}_g}$
δ_{L_a}	dL_a/dT_a
δ_{L_g}	$d\overline{L}_g/d\overline{T}_g$
δ_{PE}	$\overline{P} - \overline{E}$
ε	Fraction of total blackbody radiation
ε'	Emissivity of cloud longwave radiation
η	Θ/Θ_s
$\overline{\eta}_d$	$1 - \overline{\eta}$
Θ	Volumetric water content of the hydrologically active soil layer
Θ_o	Volumetric water content of the soil sublayer
Θ_s	Θ at saturation
λ	Roots of the characteristic equation
λ_r	Growth rate of disturbance
ρ_a	Air density
ρ_g	Soil density
ρ_w	Water density
σ	Stefan–Boltzmann constant

REFERENCES

Avissar, R., 1995: Recent advances in the representation of land–atmosphere interactions in global climate models. *Rev. Geophys.*, **33** (Suppl.), 1005–1010.

——, and Y. Liu, 1996: A three-dimensional numerical study of shallow convective clouds and precipitation induced by land-surface forcings. *J. Geophys. Res.*, **101** (D3), 7499–7518.

Betts, A. K., J. H. Ball, A. C. M. Beljaars, M. J. Miller, and P. A. Viterbo, 1996: The land–surface–atmosphere interaction: A review based on observational and global modeling perspectives. *J. Geophys. Res.*, **101** (D3), 7209–7226.

Bonan, G. B., 1994: Comparison of the land surface climatology of the NCAR CCM2 at R15 and T42 resolutions with implications for sub-grid land surface heterogeneity. *J. Geophys. Res.*, **99,** 10 357–10 364.

Castelli, F., and I. Rodriguez-Iturbe, 1995: Soil moisture–atmosphere interaction in a moist semi-geostrophic model of baroclinic instability. *J. Atmos. Sci.*, **52,** 2152–2159.

Chen, F., and R. Avissar, 1994: Impact of land–surface moisture variability on local shallow convective cumulus and precipitation in large-scale models. *J. Appl. Meteor.*, **33,** 1382–1401.

Collins, C., and R. Avissar, 1994: An evaluation with the Fourier Amplitude Sensitivity Test (FAST) of which land surface parameters are of greatest importance in atmospheric modeling. *J. Climate*, **7,** 681–703.

Cukier, R. I., C. M. Fortuin, K. E. Shuler, A. G. Petschek, and J. H. Schaibly, 1973: Study of the sensitivity of coupled reaction systems to uncertainties in rate coefficients. Part I: Theory. *J. Chem. Phys.*, **59,** 3873–3878.

——, H. B. Levine, and K. E. Shuler, 1978: Nonlinear sensitivity analysis of multiparameter model systems. *J. Comput. Phys.*, **26,** 1–42.

Delworth, T., and S. Manabe, 1988: The influence of potential evaporation on the variabilities of simulated soil wetness and climate. *J. Climate,* **1,** 523–547.

——, and ——, 1989: The influence of soil wetness on near-surface atmospheric variability. *J. Climate,* **2,** 1447–1462.

——, and ——, 1993: Climate variability and land-surface processes. *Adv. Water Resour.,* **16,** 3–20.

Derwent, R. G., 1987: Treating uncertainty in models of the atmospheric chemistry of nitrogen compounds. *Atmos. Environ.,* **21,** 1445–1454.

Dickinson, R. E., A. Henderson-Sellers, and P. J. Kennedy, 1993: Biosphere–Atmosphere Transfer Scheme (BATS) version 1E as coupled to the NCAR Community Climate Model. NCAR Tech. Note TN-387, National Center for Atmospheric Research, Boulder, CO, 72 pp.

Fu, B. P., 1978: An estimate to influence of human activities on atmospheric precipitation (in Chinese). *Proc. National Conf. on Climate Variation,* China Academic Press, 143–151.

Gao, X. G., S. Sorooshian, and H. V. Gupta, 1996: A sensitivity analysis of the Biosphere–Atmosphere Transfer Scheme (BATS). *J. Geophys. Res.,* **101** (D3), 7279–7290.

Holton, J. R., 1979: *An Introduction to Dynamic Meteorology.* Academic Press, 391 pp.

Liu, Y., and R. Avissar, 1996: Sensitivity of shallow convective precipitation induced by land surface heterogeneities to dynamical and cloud microphysical parameters. *J. Geophys. Res.,* **101** (D3), 7477–7497.

——, and ——, 1999: A study of persistence in the land–atmosphere system using a general circulation model and observations. *J. Climate,* **12,** 2139–2153.

——, D. Z. Ye, and J. J. Ji, 1992: Influence of soil moisture and vegetation on climate. Part I: A theoretical analysis on persistence of short-term climatic anomalies (in Chinese). *Sci. China,* **35B,** 441–448.

——, ——, and ——, 1993: Influence of soil moisture and vegetation on climate. Part II: Numerical experiments on persistence of short-term climatic anomalies. *Sci. China,* **36B,** 102–109.

Manabe, S., 1969: Climate and the ocean circulation. Part I: The atmospheric circulation and the hydrology of the earth's surface. *Mon. Wea. Rev.,* **97,** 739–774.

——, and T. Delworth, 1990: The temporal variability of soil wetness and its impact on climate. *Climate Change,* **16,** 185–192.

McKay, M. D., R. J. Beckman, and W. J. Conover, 1979: A comparison of three methods for selecting values of input variables in the analysis of output from a computer code. *Technometrics,* **21,** 239–245.

Namias, J., 1952: The annual course of month-to-month persistence in climatic anomalies. *Bull. Amer. Meteor. Soc.,* **33,** 279–285.

——, 1959: Persistence of mid-tropospheric circulations between adjacent months and seasons. *The Atmosphere and the Sea in Motion: Rossby Memorial Volume,* B. Bolin, Ed., Rockefeller Institute Press and Oxford University Press, 240–248.

Paltridge, G. W., 1974: Global cloud cover and earth surface temperature. *J. Atmos. Sci.,* **31,** 1571–1576.

Rind, D., 1982: The influence of ground moisture conditions in North America on summer climate as modeled in the GISS GCM. *Mon. Wea. Rev.,* **110,** 1487–1494.

Rowntree, P. R., and J. A. Bolton, 1983: Simulation of the atmospheric response to soil moisture anomalies over Europe. *Quart. J. Roy. Meteor. Soc.,* **109,** 501–526.

Uliasz, M., 1988: Application of the FAST method to analyze the sensitivity—Uncertainty of a Lagrangian model of sulphur transport in Europe. *Water, Air, Soil Pollut.,* **40,** 33–49.

Vinnikov, K., A. Robock, N. A. Speranskaya, and C. A. Schlosser, 1996: Scales of temporal and spatial variability of midlatitude soil moisture. *J. Geophys. Res.,* **101** (D3), 7163–7174.

Walker, J. M., and P. R. Rowntree, 1977: The effect of soil moisture on circulation and rainfall in a tropical model. *Quart. J. Roy. Meteor. Soc.,* **103,** 29–46.

Walsh, J. E., W. H. Jasperson, and B. Ross, 1985: Influence of snow cover and soil moisture on monthly air temperature. *Mon. Wea. Rev.,* **113,** 756–768.

Yeh, T. C., R. T. Wetherald, and S. Manabe, 1984: The effect of soil moisture on the short-term climate and hydrology change—A numerical experiment. *Mon. Wea. Rev.,* **112,** 474–490.